Geophysical Journal International

Geophys. J. Int. (2010) **183,** 237–251 doi: 10.1111/j.1365-246X.2010.04733.x

Modelling transient temperature distribution for injecting hot water through a well to an aquifer thermal energy storage system

Shaw-Yang Yang,[1] Hund-Der Yeh[2] and Kuang-Yi Li[2]

[1]*Department of Civil Engineering, Vanung University, Chungli* 320, *Taiwan*
[2]*Institute of Environmental Engineering, National Chiao Tung University, Hsinchu* 300, *Taiwan. E-mail: hdyeh@mail.nctu.edu.tw*

Accepted 2010 July 10. Received 2010 July 10; in original form 2010 February 18

SUMMARY

Heat storage systems are usually used to store waste heat and solar energy. In this study, a mathematical model is developed to predict both the steady-state and transient temperature distributions of an aquifer thermal energy storage (ATES) system after hot water is injected through a well into a confined aquifer. The ATES has a confined aquifer bounded by aquicludes with different thermomechanical properties and geothermal gradients along the depth. Consider that the heat is transferred by conduction and forced convection within the aquifer and by conduction within the aquicludes. The dimensionless semi-analytical solutions of temperature distributions of the ATES system are developed using Laplace and Fourier transforms and their corresponding time-domain results are evaluated numerically by the modified Crump method. The steady-state solution is obtained from the transient solution through the final-value theorem. The effect of the heat transfer coefficient on aquiclude temperature distribution is appreciable only near the outer boundaries of the aquicludes. The present solutions are useful for estimating the temperature distribution of heat injection and the aquifer thermal capacity of ATES systems.

Key words: Numerical solutions; Heat flow; Hydrothermal systems.

GJI Mineral physics, rheology, heat flow and volcanology

Downloaded from http://gji.oxfordjournals.org/ at National Chiao Tung University Library on April 24, 2014

1 INTRODUCTION

Conventional energy resources such as fossil fuels may produce waste heat. Therefore, waste heat stored in an appropriate aquifer is considered as a feasible and favourable way to conserve the energy. Aquifer thermal energy storage (ATES) systems provide a convenient way to store heat energy for future use. Hot water can be injected into the well, stored in geological formations, and later recovered through pumping wells. The heat recovery and storage efficiency of the ATES systems are affected by thermal losses through surface lines, injection wellbores and thermal conduction.

Bödvarsson & Tsang (1982) presented a model describing cold water injected into a reservoir with equally spaced horizontal fractures. Their model neglects the horizontal conduction and geothermal gradient of the fracture. Bödvarsson *et al*. (1982) developed a 2-D model for a fault-charged hydrothermal system considering the geothermal gradient. Their model was used to estimate the flow rate of a hydrothermal system at Susanville, California. They found that heat recovery and storage efficiency are the most important factors influencing the behaviour of the ATES system. Sauty *et al*. (1982a) presented a theoretical study on the thermal behaviour of aquifer storage for hot water. The finite difference model was used to calculate well temperature distribution over production periods. Furthermore, Sauty *et al*. (1982b) performed field experiments for hot water storage and compared the experimental data with the theoretical results of Sauty *et al*. (1982a). Chen & Reddell (1983) developed transient solutions over short and long time periods. They also proposed a steady-state solution to describe the aquifer temperature distribution after thermal injection into an aquifer bounded by rocks with the same physical properties and thicknesses. Nagano *et al*. (2002) used both observed experimental data and computer simulations to investigate the influence of natural convection on a forced horizontal flow in a ATES system. They mentioned that the performance of underground ATES is affected by the following four factors: (1) the thermal properties (e.g. thermal conductivity and thermal capacity); (2) the operating temperature range; (3) the shape and size of the storage reservoir and (4) the transient mixed convection flow. Bouhdjar & Harhad (2002) presented a numerical analysis of transient mixed convection flow in a cylindrical storage tank. Yumrutas & Ünsal (2005) developed a computer program based on an analytical model to simulate a space cooling system with underground storage. They found that higher thermal properties yield a lower storage temperature and performance value with a higher coefficient. Ghassemi & Kumar (2007) examined the changes in fracture aperture and fluid pressure resulting from the thermal stress and chemical processes induced by heat extraction from subsurface rocks. Their results show that the fluid

© 2010 The Authors
Journal compilation © 2010 RAS

flow in smaller initial fracture apertures significantly increases the fracture permeability and associated pressure drop at the injection well due to thermoporoelasticity effects.

The objective of this study is to develop a mathematical model and its corresponding solution for predicting the thermal distribution in an ATES system after recharged hot water is injected through a well into a confined aquifer. This model assumes that an injection well fully penetrates the aquifer bounded by the aquicludes with different thermomechanical properties and geothermal gradients along the depth. The outer boundaries of the aquicludes are represented by the Robin boundary conditions. Heat energy is partially stored within the aquifer and transferred by means of water flow to adjacent aquicludes. The solution in dimensionless form is developed using Laplace transforms and its corresponding results in time domain are computed by the modified Crump method (de Hoog *et al*. 1982). The solution can be applied to simulate transient temperature distributions under ATES systems and to assess the influences of thermomechanical properties on temperature distribution.

2 ANALYTICAL STUDY

2.1 Conceptual model

Fig. 1 shows a schematic representation of the ATES system. The system is comprised of the storage aquifer confined by the underlying and overlying aquicludes with different thermomechanical properties and an injection well with a finite radius fully penetrating the aquifer. Initially, both the aquifer and aquicludes are considered to have linear geothermal gradients along the vertical depth. Hot water is recharged into the aquifer and heat energy is partially transferred to the adjacent aquicludes. In the ATES system, the aquicludes are of finite thicknesses in depth and extend infinitely in the radial direction. We assume that the thermomechanical properties of the aquifer and aquicludes are temperature invariant. In addition, the thermal capacity of the aquifer, C_a, depends on the density (ρ), specific heat (c) and aquifer porosity (n), thus, it is denoted as $C_a = (\rho c)_a = n(\rho c)_{water} + (1-n)(\rho c)_{soil}$. Heat energy is transferred by horizontal conduction and thermal convection along the water flow direction within the aquifer. Vertical thermal conduction takes place along the whole aquifer thickness and the interface of the adjacent aquicludes and the aquifer. Water is injected through the well at a constant rate Q into the confined aquifer over the period of operating time and the outflow from the wellbore is uniformly distributed over the well screen. The temperature of the injected water remains constant and the initial temperature distributed over the thickness of the aquifer is specified.

Under these circumstances, the heat convection–conduction equation which describes aquifer temperature distribution can be written as

$$b_a\left[C_a\left(\frac{\partial T_a(r,z,t)}{\partial t}+u\frac{\partial T_a(r,z,t)}{\partial r}\right)-\lambda_a\left(\frac{\partial^2 T_a(r,z,t)}{\partial r^2}+\frac{1}{r}\frac{\partial T_a(r,z,t)}{\partial r}+\frac{\partial^2 T_a(r,z,t)}{\partial z^2}\right)\right]$$
$$=-\lambda_1\frac{\partial T_1(r,z,t)}{\partial z}\Big|_{z=0}+\lambda_2\frac{\partial T_2(r,z,t)}{\partial z}\Big|_{z=b_a}, \quad (1)$$

where the subscripts a, 1 and 2 denote the aquifer, the underlying aquiclude and overlying aquiclude, respectively; T is the temperature; λ is the thermal conductivity; b is the thickness; C is the thermal capacity; z is the vertical distance from the bottom of the aquifer; r is the radial distance from the centre of the injection well and t is the operating time. (See Table C1 for a list of all the notations used in this paper.) The flow velocity within the aquifer (u) is equal to $Q/(2\pi r n b_a)$, where n is the aquifer porosity and Q is a constant injection rate.

The initial temperature of the aquifer is

$$T_a(r,z,0) = T_{a0} - g_a z, \quad 0 < z < b_a, \quad (2)$$

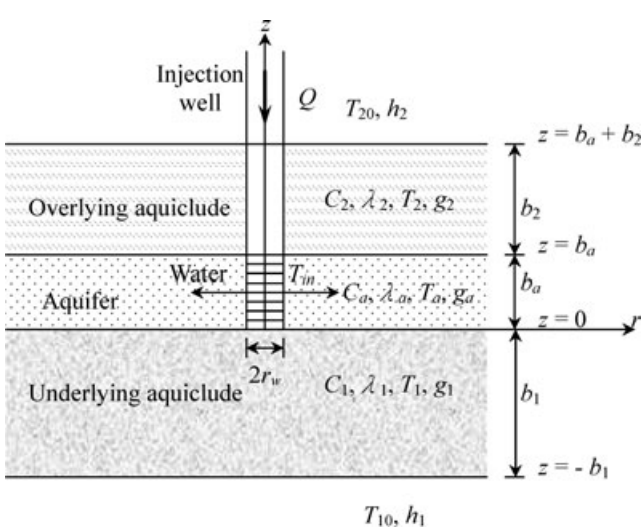

Figure 1. Schematic representation of an aquifer thermal energy storage system.

Downloaded from http://gji.oxfordjournals.org/ at National Chiao Tung University Library on April 24, 2014

where g_a is the geothermal gradient of the aquifer and T_{a0} is the constant temperature at the middle part of the aquifer. The boundary conditions at the injection well and the infinite distance from the injection well are, respectively,

$$T_a(r_w, z, t) = T_{in} \tag{3}$$

and

$$T_a(\infty, z, t) = T_{a0} - g_a z, \;\; 0 < z < b_a, \tag{4}$$

where T_{in} is a constant temperature of the injection water and r_w is the radius of the injection well.

The boundary conditions at the interface of the underlying and overlying aquicludes are, respectively,

$$\frac{\partial T_a(r, 0, t)}{\partial z} = \frac{\partial T_1(r, 0, t)}{\partial z} \tag{5}$$

and

$$\frac{\partial T_a(r, b_a, t)}{\partial z} = \frac{\partial T_2(r, b_a, t)}{\partial z}. \tag{6}$$

The heat conduction equation describing the temperature distribution in the underlying aquiclude can be written as

$$\frac{\partial^2 T_1(r, z, t)}{\partial z^2} = \frac{C_1}{\lambda_1}\frac{\partial T_1(r, z, t)}{\partial t} \tag{7}$$

subject to the following initial and boundary conditions

$$T_1(r, z, 0) = T_{a0} - g_1 z, \;\; -b_1 < z < 0 \tag{8}$$

$$T_1(r, 0, t) = T_a(r, z, t) \;\; \text{for the upper boundary} \tag{9}$$

and

$$-\frac{\partial T_1(r, -b_1, t)}{\partial z} = -\frac{h_1}{\lambda_1}\left[T_1(r, -b_1, t) - T_{10}\right] \;\; \text{for the lower boundary} \tag{10}$$

where g_1 is the geothermal gradient of the underlying aquiclude; h_1 is the heat transfer coefficient of the lower underlying aquiclude and T_{10} is the surface temperature of the lower underlying aquiclude, $T_{10} = T_{a0} + g_1 b_1$.

The heat conduction equation describing the temperature distribution in the overlying aquiclude can be written as

$$\frac{\partial^2 T_2(r, z, t)}{\partial z^2} = \frac{C_2}{\lambda_2}\frac{\partial T_2(r, z, t)}{\partial t} \tag{11}$$

subject to the following initial and boundary conditions

$$T_2(r, z, 0) = T_{a0} - g_2 z, \;\; b_a < z < b_a + b_2 \tag{12}$$

$$T_2(r, b_a, t) = T_a(r, z, t) \;\; \text{for the lower boundary} \tag{13}$$

and

$$-\frac{\partial T_2(r, b_a + b_2, t)}{\partial z} = \frac{h_2}{\lambda_2}\left[T_2(r, b_a + b_2, t) - T_{20}\right] \;\; \text{for the upper boundary} \tag{14}$$

where g_2 is the geothermal gradient of the overlying aquiclude; h_2 is the heat transfer coefficient of the upper overlying aquiclude and T_{20}, the surface temperature of the upper overlying aquiclude, can be expressed as $T_{20} = T_{a0} - g_2(b_a + b_2)$.

2.2 Laplace-domain solutions

Using the normalized parameters listed in Table 1, eqs (1)–(14) can be expressed in dimensionless forms. The detailed developments of the Laplace-domain solutions for the dimensionless temperature distributions in the aquifer, underlying- aquiclude and overlying-aquiclude are given in Appendix A. The final result of dimensionless aquifer temperature distribution in the Laplace domain is

$$\bar{T}_{aD}(R, Z_a, p) = \frac{1}{2}\bar{T}^*_{aD}(R, 0, p) + \sum_{n=1}^{\infty}\bar{T}^*_{aD}(R, \zeta_a, p)\cos(\zeta_a Z_a), \;\; \zeta_a = \frac{n\pi}{2} \tag{15}$$

Table 1. Normalized parameters used in the study.

$T_{aD}(R, Z_a, \tau) = \frac{T_a(r,z,t)-T_{a0}}{T_{in}-T_{a0}}$, $T_{1D}(R, Z_1, \tau) = \frac{T_1(r,z,t)-T_{a0}}{T_{in}-T_{a0}}$, $T_{2D}(R, Z_2, \tau) = \frac{T_2(r,z,t)-T_{a0}}{T_{in}-T_{a0}}$
$T_{10D} = \frac{T_{10}-T_{a0}}{T_{in}-T_{a0}}$, $T_{20D} = \frac{T_{20}-T_{a0}}{T_{in}-T_{a0}}$, $T_{ag} = \frac{g_a b_a}{4(T_{in}-T_{a0})}$, $T_{1g} = \frac{g_1 b_a}{4(T_{in}-T_{a0})}$, $T_{2g} = \frac{g_2 b_a}{4(T_{in}-T_{a0})}$
$R = \frac{2r}{b_a}$, $R_w = \frac{2r_w}{b_a}$, $Z_a = \frac{2z}{b_a}$, $Z_1 = -\frac{4z}{b_a}$, $Z_2 = \frac{4(z-b_a)}{b_a}$, $\tau = \frac{4\alpha_a t}{b_a^2}$, $w = \frac{QC_a}{4\pi n b_a \lambda_a}$
$B_1 = \frac{b_1}{b_a}$, $B_2 = \frac{b_2}{b_a}$, $\lambda_{1D} = \frac{\lambda_1}{\lambda_a}$, $\lambda_{2D} = \frac{\lambda_2}{\lambda_a}$
$\alpha_{1D} = \frac{4\alpha_1}{\alpha_a}$, $\alpha_{2D} = \frac{4\alpha_2}{\alpha_a}$, $\beta_1 = \frac{h_1 b_a}{\lambda_1}$, $\beta_2 = \frac{h_2 b_a}{\lambda_2}$

Downloaded from http://gji.oxfordjournals.org/ at National Chiao Tung Unive [redacted] on April 24, 2014

with

$$\bar{T}^{*}_{aD}(R,\zeta_a,p)=\frac{1}{p}\left(\frac{R}{R_w}\right)^{v}\left[\frac{K_v\left(\sqrt{A(\zeta_a,p)}R\right)}{K_v\left(\sqrt{A(\zeta_a,p)}R_w\right)}\right]\left[\frac{B(\zeta_a,p)}{A(\zeta_a,p)}+\frac{\sin(2\zeta_a)}{\zeta_a}\right]-\frac{B(\zeta_a,p)}{pA(\zeta_a,p)} \tag{16}$$

$$A(\zeta_a,p)=p+\lambda_{1D}q_1x_1+\lambda_{2D}q_2x_2+\zeta_a^2 \tag{17}$$

and

$$B(\zeta_a,p)=\frac{\sin(2\zeta_a)\alpha(p)}{\zeta_a}-(-1)^n\left[\beta(p)-2T_{2g}\right]+\frac{2pT_{ag}}{\zeta_a^2}\left[2\zeta_a\sin(2\zeta_a)+\cos(2\zeta_a)-1\right]-2q_1y_1a_1-2T_{1g}, \tag{18}$$

where p and ζ are the Laplace and Fourier variables, respectively (Spiegel 1965); $K_v(\cdot)$ is the modified Bessel function of the second kind with order v, $QC_a/4\pi nb_a\lambda_a$; $q_1^2=p/\alpha_{1D}$; $q_2^2=p/\alpha_{2D}$; $a_1=\beta_1T_{10D}-4T_{1g}(1+\beta_1B_1)$; $a_2=\beta_2T_{20D}+4T_{2g}(1+\beta_2+\beta_2B_2)$; $\alpha(p)=-q_1\lambda_{1D}y_1a_1-q_2\lambda_{2D}y_2a_2-\lambda_{1D}T_{1g}+\lambda_{2D}T_{2g}+4q_2\lambda_{2D}T_{2g}x_2$; $\beta(p)=2q_2y_2a_2\big/(1+4q_2x_2)$; $y_i=1/[4q_i\cosh(4q_iB_i)+\beta_i\sinh(4q_iB_i)]$ and $x_i=y_i[4q_i\sinh(4q_iB_i)+\beta_i\cosh(4q_iB_i)]$, where $i=1,2$. In addition, the Laplace-domain solutions of dimensionless temperature distribution in the underlying and overlying aquicludes are, respectively,

$$\begin{aligned}\bar{T}_{1D}(R,Z_1,p)=&\,\overline{T}_{aD}(R,Z_a,p)\,y_1\{4q_1\cosh[q_1(4B_1-Z_1)]+\beta_1\sinh[q_1(4B_1-Z_1)]\}\\&+\frac{\sinh(q_1Z_1)\,y_1}{p}\left[\beta_1T_{10D}-4T_{1g}(1+\beta_1B_1)\right]+\frac{T_{1g}}{p}Z_1\end{aligned} \tag{19}$$

and

$$\begin{aligned}\bar{T}_{2D}(R,Z_2,p)=&\left(\overline{T}_{aD}(R,Z_a,p)+\frac{4T_{2g}}{p}\right)y_2\{4q_2\cosh[q_2(4B_2-Z_2)]+\beta_2\sinh[q_2(4B_2-Z_2)]\}\\&+\frac{\sinh(q_2Z_2)\,y_2}{p}\left[\beta_2T_{20D}+4T_{2g}(1+\beta_2+\beta_2B_2)\right]-\frac{T_{2g}}{p}(Z_2+4).\end{aligned} \tag{20}$$

For a thin aquifer, the geothermal gradient does not significantly affect the dimensionless aquifer temperature distribution, therefore, eq. (15) can be simplified as

$$\bar{T}_{aD}\left(R,\frac{b_a}{2},p\right)=\frac{1}{p}\left(\frac{R}{R_w}\right)^{v}\left[\frac{K_v\left(\sqrt{A(0,p)}R\right)}{K_v\left(\sqrt{A(0,p)}R_w\right)}\right]\left[1+\frac{B(0,p)}{A(0,p)}\right]-\frac{B(0,p)}{pA(0,p)},\quad \zeta_a=0 \tag{21}$$

with

$$A(0,p)=p+\lambda_{1D}q_1x_1+\lambda_{2D}q_2x_2 \tag{22}$$

and

$$B(0,p)=-q_1y_1a_1(\lambda_{1D}+1)-q_2y_2a_2\left[\lambda_{2D}+1\big/(1+4q_2x_2)\right]-(\lambda_{1D}+1)T_{1g}+(\lambda_{2D}+1)T_{2g}+4q_2\lambda_{2D}T_{2g}x_2. \tag{23}$$

The geothermal gradients in the aquicludes equal zero if the initial temperature distributions in the underlying and overlying aquicludes are uniform; that is, $g_1=g_2=0$. In addition, in the ATES system no heat transfer is assumed at the outer boundaries of the underlying and overlying aquicludes, and the values of dimensionless parameters T_{1g}, T_{2g}, β_1, β_2 and $B(p)$ are then all equal to zero. Thus, the Laplace-domain solutions of eqs (19)–(21) in dimensionless forms are, respectively, reduced to

$$\bar{T}_{1D}(R,Z_1,p)=\frac{\cosh[q_1(4B_1-Z_1)]}{\cosh(4q_1B_1)}\bar{T}_{aD}\left(R,\frac{b_a}{2},p\right) \tag{24}$$

$$\bar{T}_{2D}(R,Z_2,p)=\frac{\cosh[q_2(4B_2-Z_2)]}{\cosh(4q_2B_2)}\bar{T}_{aD}\left(R,\frac{b_a}{2},p\right) \tag{25}$$

and

$$\bar{T}_{aD}\left(R,\frac{b_a}{2},p\right)=\frac{1}{p}\left(\frac{R}{R_w}\right)^{v}\left[\frac{K_v\left(\sqrt{A'(0,p)}R\right)}{K_v\left(\sqrt{A'(0,p)}R_w\right)}\right], \tag{26}$$

where $A'(0,p)=p+\lambda_{1D}q_1\tanh(4q_1B_1)+\lambda_{2D}q_2\tanh(4q_2B_2)$. The above equations are the Laplace-domain solutions for dimensionless temperature distribution within the aquifer and the underlying and overlying aquicludes. These solutions do not consider the geothermal gradient and heat transfer coefficient.

2.3 Steady-state solution

For an infinite operating time, thermal energy transfer from the aquifer to the aquicludes in the ATES system is zero at any radial distance r. The steady-state solution of dimensionless aquifer temperature can then be obtained from eq. (15) by applying the final-value theorem

Downloaded from http://gji.oxfordjournals.org/ at National Chiao Tung University Library on April 24, 2014

(Yeh & Wang 2007). The development of the steady-state solution for dimensionless aquifer temperature distribution in the time domain is developed in detail in Appendix B and the result is

$$T_{aD}(R, Z_a, \infty) = \frac{1}{2} T^*_{aD}(R, 0, \infty) + \sum_{n=1}^{\infty} T^*_{aD}(R, \zeta_a, \infty) \cos(\zeta_a Z_a), \quad \zeta_a = \frac{n\pi}{2} \tag{27}$$

with

$$T^*_{aD}(R, \zeta_a, \infty) = \left(\frac{R}{R_w}\right)^v \left[\frac{K_v\left(\sqrt{A(\zeta_a, 0)}R\right)}{K_v\left(\sqrt{A(\zeta_a, 0)}R_w\right)}\right]\left[\frac{B(\zeta_a, 0)}{A(\zeta_a, 0)} + \frac{\sin(2\zeta_a)}{\zeta_a}\right] - \frac{B(\zeta_a, 0)}{A(\zeta_a, 0)}.$$

The steady-state solution of eq. (21) in the time domain for the thin aquifer is

$$T_{aD}\left(R, \frac{b_a}{2}, \infty\right) = \left(\frac{R}{R_w}\right)^v \left[\frac{K_v\left(\sqrt{A(0, 0)}R\right)}{K_v\left(\sqrt{A(0, 0)}R_w\right)}\right]\left[1 + \frac{B(0, 0)}{A(0, 0)}\right] - \frac{B(0, 0)}{A(0, 0)}, \tag{28}$$

where $x = 1/(4 + 4\beta_1 B_1)$, $y = 1/(4 + 4\beta_2 B_2)$, $A(0, 0) = \lambda_{1D}\beta_1 x + \lambda_{2D}\beta_2 y$ and $B(0, 0) = -xa_1(\lambda_{1D} + 1) - ya_2\left[\lambda_{2D} + 1/(1 + 4\beta_2 y)\right] - (\lambda_{1D} + 1)T_{1g} + (\lambda_{2D} + 1)T_{2g} + 4\lambda_{2D}T_{2g}\beta_2 y$.

Similarly, the steady-state solutions of dimensionless temperature distribution in the underlying and overlying aquicludes can be obtained from eqs (19) and (20), respectively. They are

$$T_{1D}(R, Z_1, \infty) = T_{aD}\left(R, \frac{b_a}{2}, \infty\right)(1 - \beta_1 Z_1 x) + T_{10D}\beta_1 Z_1 x \tag{29}$$

and

$$T_{2D}(R, Z_2, \infty) = T_{aD}\left(R, \frac{b_a}{2}, \infty\right)(1 - \beta_2 Z_2 y) + T_{20D}\beta_2 Z_2 y \tag{30}$$

3 NUMERICAL INVERSION FOR LAPLACE-DOMAIN SOLUTIONS

Eqs (15), (19) and (20) comprise hyperbolic functions [i.e. sinh(·) and cosh(·)] and Bessel function $K_w(\cdot)$; thus their time-domain solutions may not be tractable. The inversion routine DINLAP of IMSL (2003), developed based on a numerical algorithm originally proposed by Crump (1976) and later modified by de Hoog *et al*. (1982), is used to obtain the time-domain solution. This routine has been successfully applied to solve some groundwater problems (see, e.g. Chen *et al*. 1996; Yeh & Yang 2006). This algorithm approximates Laplace inversion in a Fourier series and accelerates the computation using the Shanks method (Shanks 1955). Eqs (15), (19) and (20) are numerically inverted using this routine with accuracy to the fourth decimal.

The Bessel function of $K_v(\varepsilon)$ included in eqs (15), (19) and (20) is non-integral and depends on dimensionless convective parameter v. Using an ascending series for $I_v(\varepsilon)$, the term $K_v(\varepsilon)$ given by Abramowitz & Stegun (1964, p. 375) can be written as

$$K_v(\varepsilon) = \frac{\pi}{2}\frac{I_{-v}(\varepsilon) - I_v(\varepsilon)}{\sin(v\pi)} \tag{31}$$

with

$$I_v(\varepsilon) = \left(\frac{\varepsilon}{2}\right)^v \sum_{k=0}^{\infty} \frac{\left(\frac{1}{4}\varepsilon^2\right)^k}{k!\Gamma(v + k + 1)}, \tag{32}$$

where $\Gamma(\cdot)$ is the Gamma function. As $|\varepsilon|$ is large, $K_v(\varepsilon)$ tends to infinity. Using asymptotic expansion for a large argument, $K_v(\varepsilon)$ can be approximated as (1964, p. 378)

$$K_v(\varepsilon) = \sqrt{\frac{\pi}{2\varepsilon}}e^{-\varepsilon}\left\{1 + \frac{\delta - 1}{8\varepsilon} + \frac{(\delta - 1)(\delta - 9)}{2!(8\varepsilon)^2} + \frac{(\delta - 1)(\delta - 9)(\delta - 25)}{3!(8\varepsilon)^3} + \ldots\right\}, \left(|\arg\varepsilon| < \frac{3}{2}\pi\right), \tag{33}$$

where $\delta = 4v^2$. The evaluation of eq. (33) is tedious and laborious. The Shanks method is adopted to accelerate the computation of the infinite sum in this equation. This method had been successfully applied to efficiently compute solutions in groundwater area (e.g. Yang *et al.* 2006; Yang & Yeh 2007).

4 RESULTS AND DISCUSSION

The injection well has a finite radius r_w of 0.05 m and the injection rate Q of 10^{-4} m^3 s^{-1} is considered. The aquifer thickness b_a is 50 m and the thicknesses of the underlying and overlying aquicludes, that is, b_1 and b_2, are 100 and 75 m, respectively. Hot water with a uniformly constant temperature T_{in} of 70 °C is recharged into the aquifer with an initial temperature T_{a0} of 30.5 °C at the middle part of the aquifer (i.e. at $z = 25$ m). The field data of Bödvarsson & Tsang (1982) are adopted in the case study and the thermal properties of the aquifer and aquicludes are listed in Table 2.

© 2010 The Authors, *GJI*, **183,** 237–251
Journal compilation © 2010 RAS

Downloaded from http://gji.oxfordjournals.org/ at National Chiao Tung Unive[redacted] on April 24, 2014

Table 2. Parameter values of the aquifer and adjacent aquicludes.

Parameter name	Symbol	Value
Thickness of the aquifer	b_a	50 m
Thickness of the aquicludes	b_1, b_2	100, 75 m
Volumetric thermal capacity of the aquifer	C_a	2.695×10^6 J (m^3 K)$^{-1}$
Volumetric thermal capacity of the underlying aquiclude	C_1	2.7×10^6 J (m^3 K)$^{-1}$
Volumetric thermal capacity of the overlying aquiclude	C_2	2.65×10^6 J (m^3 K)$^{-1}$
Thermal conductivity of the aquifer	λ_a	2.4 W (m K)$^{-1}$
Thermal conductivity of the aquicludes	λ_1, λ_2	1.5, 2.0 W (m K)$^{-1}$
Heat transfer coefficient of the aquicludes	h_1, h_2	1.0, 0.6 W (m^2 K)$^{-1}$
Geothermal gradient of the aquifer	g_a	0.02°C m^{-1}
Geothermal gradient of the aquicludes	g_1, g_2	0.02, 0.02°C m^{-1}
Porosity of the aquifer	n	0.3

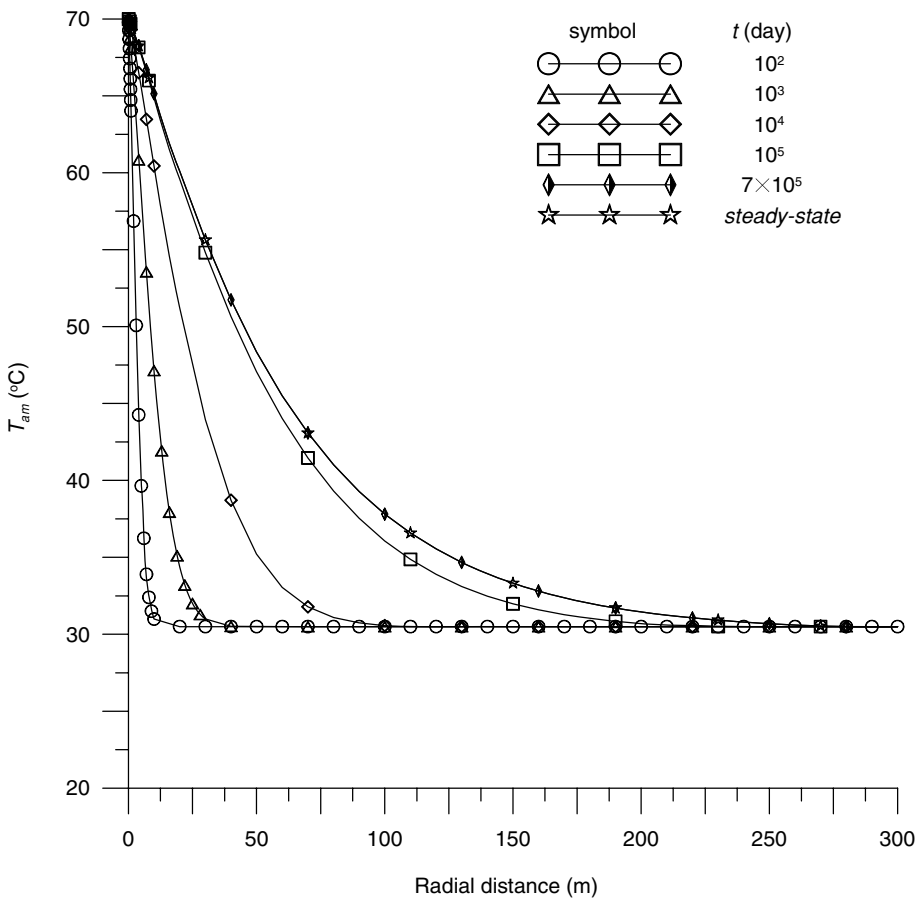

Figure 2. Distribution curves of aquifer temperature at $z = 25$ m (T_{am}) versus radial distance (r) predicted by the transient solution at $t = 10^2$, 10^3, 10^4, 10^5 and 7×10^5 d, and the steady-state solution for $C_a = 2.695 \times 10^6$ J (m^3 K)$^{-1}$, $\lambda_a = 2.4$ W (m K)$^{-1}$, $b_a = 50$ m, $T_{in} = 70$ °C, $T_{a0} = 30.5$ °C at the middle part of the aquifer and $Q = 10^{-4}$ m^3 s^{-1} in the ATES system.

The temperature profiles at $z = 25$ m (denoted as T_{am}) versus the radial distance (r) are shown in Fig. 2 for various operating periods (namely, $t = 10^2$, 10^3, 10^4, 10^5 and 7×10^5 d). This figure shows that the T_{am} generally increases with t near the injection well. At the same t, the T_{am} decreases with increasing r and approaches the T_{a0} at a large r. The relative difference in the T_{am} between the steady-state solution and the transient solution at $t = 10^5$ d is about 1.19 per cent. The T_{am} at 10^5 d compared with that at 7×10^5 d is about 0.5 °C smaller for $r \leq 20$ m and produces a maximum difference of 1.74 °C at $r = 95$ m. This figure also shows that the temperature predicted for the middle part of the aquifer by the transient solution at $t = 7 \times 10^5$ d is identical to that of the steady-state solution.

The efficiency of energy storage in the ATES system is affected by aquifer thickness (b_a), aquifer thermal conductivity (λ_a) and injection flow rate (Q). Fig. 3 demonstrates the spatial temperature distributions at the middle part of the aquifer at $t = 100$ d predicted by the present solution, eq. (15), and a simplified solution, eq. (20), for chosen values of b_a, λ_a and Q. The effect of aquifer thickness on aquifer temperature can be observed from Fig. 3 for the cases with $\lambda_a = 2.4$ W (m K)$^{-1}$ and $Q = 10^{-4}$ m^3 s^{-1} when $b_a = 50$ m (case 1) or 20 m (case 2). This figure shows that a larger b_a yields a smaller T_{am} at the same radial distance r. However, both temperature distribution curves approach different constant values at $r = 15$ m due to the effects of the geothermal gradient and vertical conduction. The difference in T_{am} between these two

Downloaded from http://gji.oxfordjournals.org/ at National Chiao Tung University Library on April 24, 2014

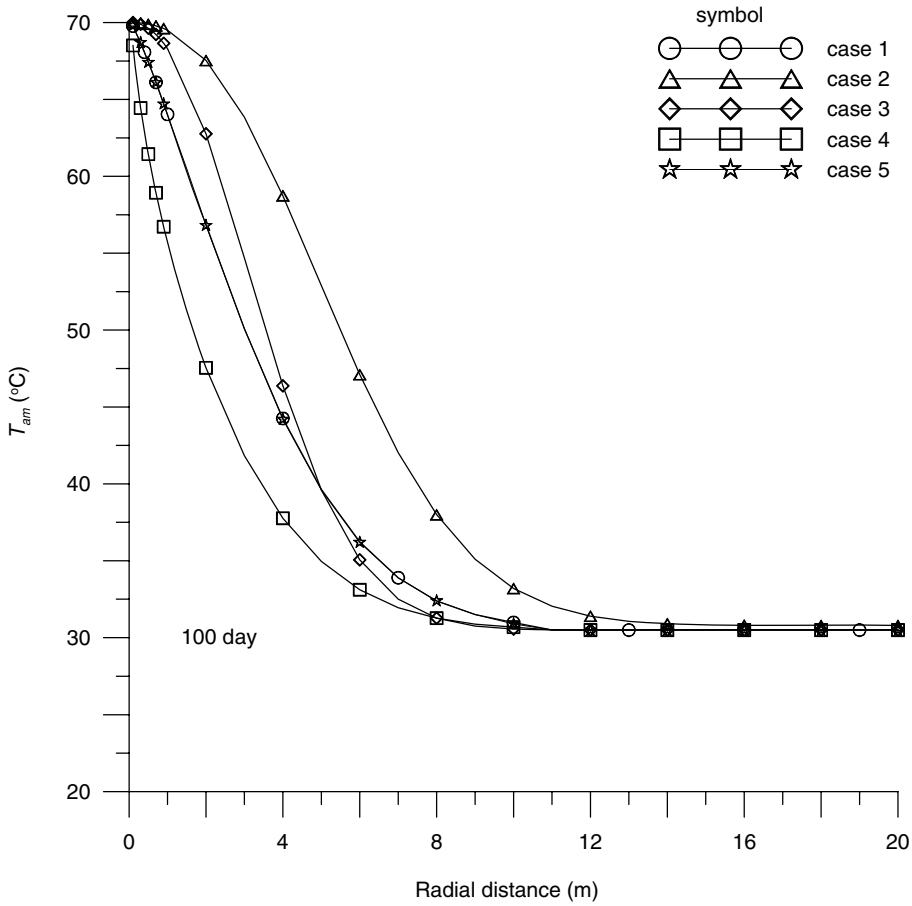

Figure 3. Distribution curves of aquifer temperature at $z = 25$ m (T_{am}) versus radial distance (r) at the time period of 100 d for different values of aquifer thickness in case 2, aquifer thermal conductivity in case 3, injection flow rate in case 4 and the simplified solution in case 5.

cases increases with r, gives the maximum value at about $r = 4$ m, and then decreases with r, indicating that heat storage capacity increases with aquifer thickness. When $b_a = 50$ m and $Q = 10^{-4}$ m^3 s^{-1}, it is shown that T_{am} in the case 1 is smaller at small r, the same at about $r = 5$ m and larger after about $r = 5$ m than that in the case with $\lambda_a = 1.2$ W (m K)$^{-1}$ (case 3). In addition, both temperature distribution curves approach almost the same value after $r = 10$ m. For $b_a = 50$ m and $\lambda_a = 2.4$ W (m K)$^{-1}$, the effect of the injection flow rate on T_{am} is further reviewed in Fig. 3 for case 1 (with $Q = 10^{-4}$ m^3 s^{-1}) and the case with 5×10^{-5} m^3 s^{-1} (case 4). The figure shows that a greater Q produces a higher T_{am}. Both T_{am} curves approach the same value at about $r = 10$ m, indicating that the heat storage capacity increases with injection flow rate. Obviously, the aquifer thermal properties and injection flow rate play an important role in affecting the temperature distribution in ATES systems. In addition, the predicted curve of T_{am} versus r by the simplified solution designated as case 5, neglecting the vertical geothermal gradient of the aquifer, is displayed in Fig. 3 for $b_a = 50$ m, $\lambda_a = 2.4$ W (m K)$^{-1}$ and $Q = 10^{-4}$ m^3 s^{-1}. The result shows that the T_{am} estimated for case 5 is almost identical to that of case 1. The temperatures predicted by these two solutions approach the initial aquifer temperature T_{a0} of 30.5 °C at about $r = 11$ m, indicating that the effect of the vertical geothermal gradient in the aquifer on temperature distribution is almost negligible.

Consider the parameter values $C_a = 2.695 \times 10^6$ J (m^3 K)$^{-1}$, $\lambda_a = 2.4$ W (m K)$^{-1}$ and $b_a = 50$ m for the aquifer and $C_1 = C_2 = 2.65 \times 10^6$ J (m^3 K)$^{-1}$, $\lambda_1 = \lambda_2 = 2.0$ W (m K)$^{-1}$ and $b_1 = b_2 = 100$ m for the adjacent aquicludes. The heat recovery ratio, defined as the recovered heat energy (enthalpy) of the water from the aquifer divided by the recharged heat energy of the water to the aquifer, is calculated herein for the design of the ATES system. Fig. 4 shows the curves of heat recovery ratio (η) at $z = 25$ m versus operating time (t) plotted based on the present solution denoted as a solid line. The Chen & Reddell solution (CRS) (1983) is denoted as a dashed line for r ranging from 1 to 40 m when t is from 10 to 10^6 d. This indicates that the η increases with increasing t and decreasing r. In addition, the present solution has a higher η than the CRS at the same t. The differences between the present solution and the CRS increase with r and approach constant values at large t. The results show that the CRS underestimates the heat recovery ratio because the aquifer porosity and geothermal gradient are neglected in the CRS.

Fig. 5 shows the contour of temperature distribution in the ATES system at $t = 100$ d. Consider that this ATES system has no heat loss at the interface between the aquifer and aquicludes and heat transfer takes place at both the bottom of the underlying aquiclude and the top of the overlying aquiclude. In this study, the radius of influence of the temperature is defined as the distance from the injection well to a

© 2010 The Authors, *GJI*, **183,** 237–251
Journal compilation © 2010 RAS

Downloaded from http://gji.oxfordjournals.org/ at National Chiao Tung Unive[redacted] on April 24, 2014

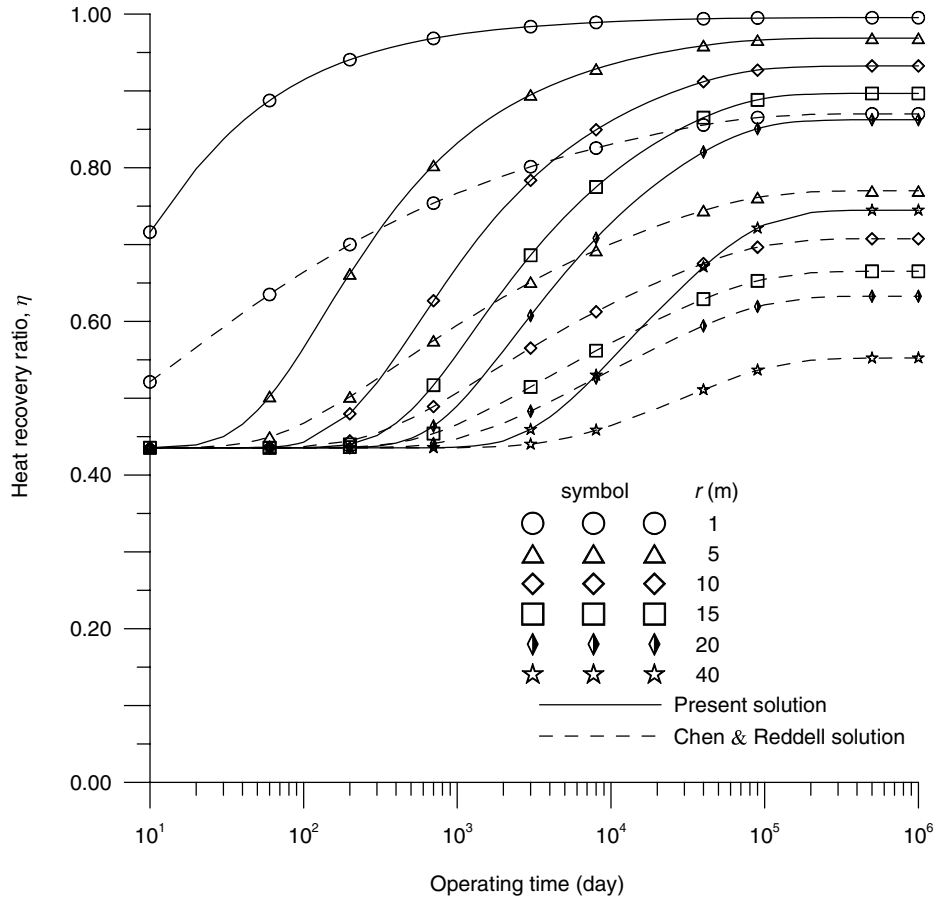

Figure 4. The curves of heat recovery ratio (η) at $z = 25$ m versus operating time (t) for r ranging from 1 m to 40 m when t is from 10 to 10^6 d. The dashed line represents the Chen & Reddell (1983) solution and the solid line represents the present solution.

location where the temperature is 0.5 °C higher than the initial temperature at the middle part of the aquifer. Fig. 5 demonstrates that the radii of influence are located at $r = 9.0$ m in the aquifer and $z = -8.2$ and 57.5 m in the underlying and overlying aquicludes, respectively.

The effects of heat transfer coefficient (h) and operating time (t) on temperature distribution are also investigated. Fig. 6 shows the profiles of temperature versus vertical distance for $r = 1$ m, $h_1 = h_2 = 0$ (no heat transferred) and 1.0 W (m^2 K)$^{-1}$ when $t = 360$ or 10^3 d. The causes of the non-uniformly distributed temperature near the outer boundaries of the underlying and overlying aquicludes are attributed to the difference of the Biot number, $\beta_i = h_i b_a / \lambda_i$, where $i = 1, 2$. When $\beta < 0.1$, the temperature distribution in the aquiclude is uniform and the heat energy can be transferred rapidly throughout the aquiclude. The temperature distribution in the aquiclude is non-uniform if $\beta > 0.1$ (Özisik 1993, p. 29). For the cases of $h_1 = h_2 = 0$ and 1.0 W (m^2 K)$^{-1}$, $\beta's$ are then 0 and 33.3, respectively, at the underlying aquiclude boundary and 0 and 25, respectively, at the overlying aquiclude boundary. Therefore, the effects of h at the outer boundaries of the underlying and overlying aquicludes must be considered in the case of $\beta > 0.1$. Fig. 6 shows that the temperature distributions in the overlying aquiclude for the cases of $h_1 = h_2 = 0$ and 1.0 W (m^2 K)$^{-1}$ are the same and dramatically decrease with increasing vertical distance before $z = 58$ m and then slowly between 58 m $\leq z \leq$ 65 m at $t = 360$ d. However, the temperature for the case of $h_1 = h_2 = 1.0$ W (m^2 K)$^{-1}$ is slightly lower than that for the case of $h_1 = h_2 = 0$ W/(m^2 K)$^{-1}$ after $z > 58$ m. In addition, the higher the h the lower the temperature along the vertical distance, especially near the upper boundary. The temperature distributions in the underlying aquiclude are, to some degree, close to those within the overlying aquiclude. The temperature distributions for the cases of $h_1 = h_2 = 0$ and 1.0 W (m^2 K)$^{-1}$ are the same and obviously decrease with increasing vertical distance bellow $z = 0$ m and then slowly decrease between -10 m $\leq z \leq -20$ m. However, the temperature distributions for the $h_1 = h_2 = 1.0$ W (m^2 K)$^{-1}$ case are higher than those for the $h_1 = h_2 = 0$ W (m^2 K)$^{-1}$ case after $z > -10$ m. These results indicate that the effect of heat transfer coefficient on aquiclude temperature is significant only near the outer boundaries of the underlying and overlying aquicludes. The temperature distribution at $t = 10^3$ d, as shown in Fig. 6, is different from that at $t = 360$ d. The temperatures of the underlying and overlying aquicludes near the aquifer at $t = 10^3$ d are higher than those at $t = 360$ d. However, the effect of h on aquiclude temperature increases with t. These results indicate that the effect of the heat transfer coefficient on aquiclude temperature distribution is appreciable only near the outer boundaries of the underlying and overlying aquicludes and increases with operating time.

Downloaded from http://gji.oxfordjournals.org/ at National Chiao Tung University Library on April 24, 2014

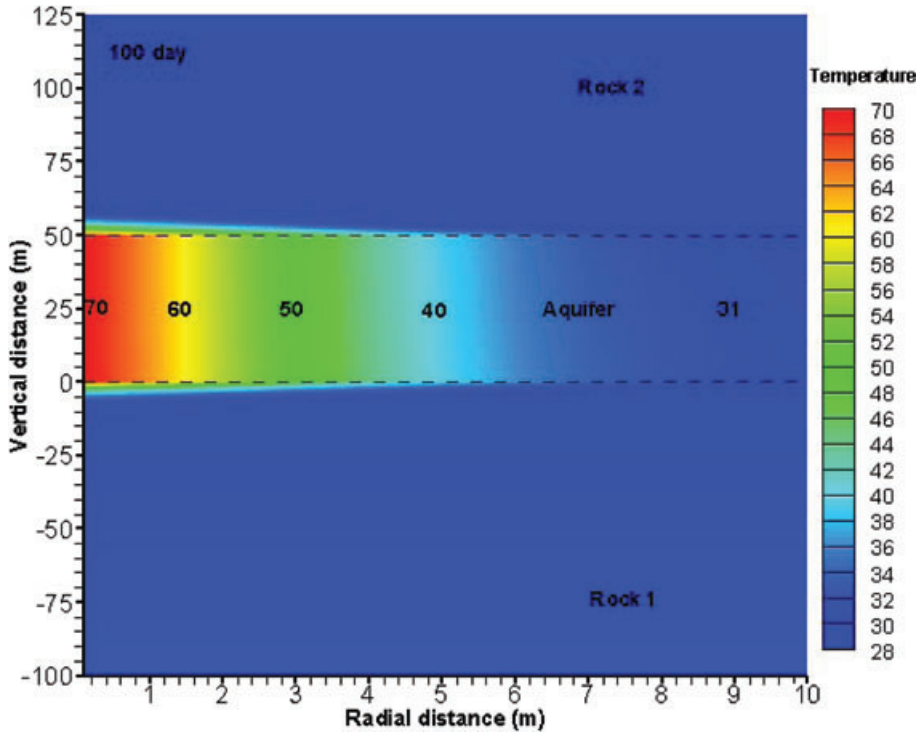

Figure 5. The contour of temperature distribution in the ATES system for $h_1 = 1.0$ W (m^2 K)$^{-1}$ and $h_2 = 0.6$ W (m^2 K)$^{-1}$ at $t = 100$ d.

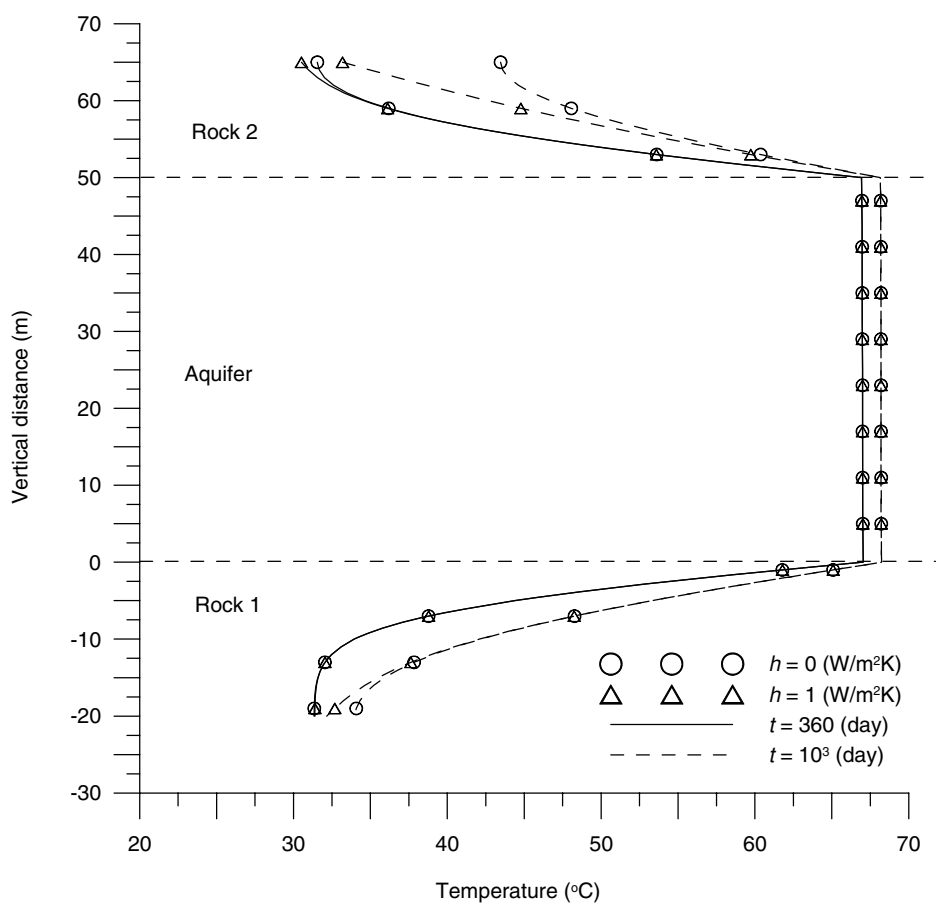

Figure 6. Isothermal plots of the aquifer and aquicludes versus vertical distance z for $r = 1$ m and $h_1 = h_2 = 0$ and 1.0 W (m^2 K)$^{-1}$ when $t = 360$ or 10^3 d.

© 2010 The Authors, *GJI*, **183,** 237–251
Journal compilation © 2010 RAS

Downloaded from http://gji.oxfordjournals.org/ at National Chiao Tung Unive[redacted] on April 24, 2014

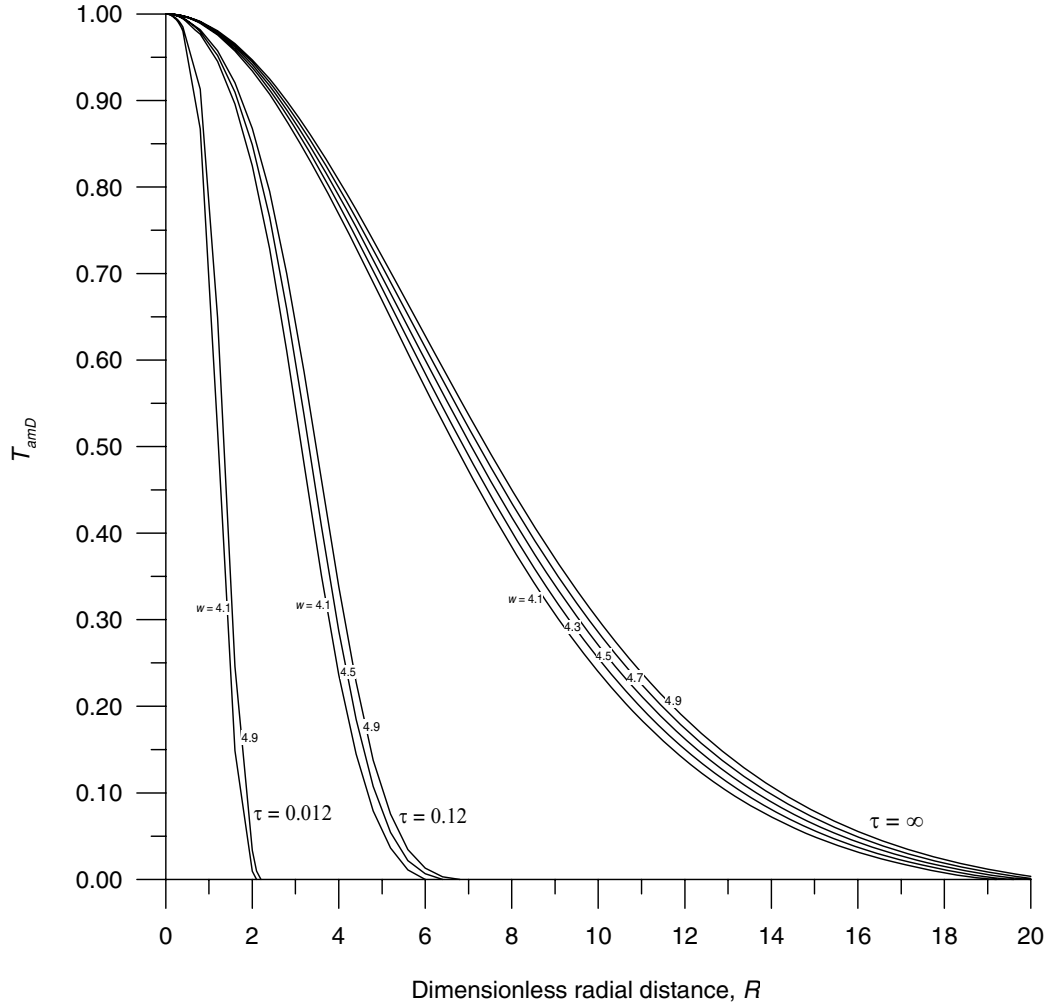

Figure 7. Type curves of dimensionless aquifer temperature (T_{am}) at $z = 25$ m versus dimensionless radial distance for w ranging from 4.1 to 4.9 at $\tau = 0.012$ (10^3 d), 0.12 (10^4 d) and infinity.

The type curves of the dimensionless aquifer temperature of T_{am} at $z = 25$ m versus dimensionless radial distance are plotted in Fig. 7 when the w ranges from 4.1 to 4.9 and the dimensionless time τ is at 0.012 (10^3 d), 0.12 (10^4 d), and infinity. This figure can be considered to represent different type curves for the estimation of the aquifer parameters such as thermal conductivity and thermal capacity.

5 CONCLUSIONS

A mathematical model is developed to simulate thermal distribution when hot water is recharged into the confined aquifer through an injection well in an ATES system. Semi-analytical solutions for describing the dimensionless temperature distribution in the aquifer and its underlying and overlying aquicludes have been presented. The time-domain results are computed numerically using the modified Crump method and presented graphically with the steady-state solution. In addition, the type curves of dimensionless aquifer temperature versus dimensionless radial distance for various dimensionless convective parameters are also provided. The results obtained from the present solutions have revealed several important points. A smaller aquifer thickness and/or larger injection hot flow rate yield a larger aquifer temperature. The temperatures within the aquifer and aquicludes increase with thermal conductivity. On the other hand, they decrease with increasing radial and vertical distances. The comparison of the present solution with the CRS indicates that the present solution predicts higher heat recovery ratio than the CRS at the same operating time. This is mainly due to fact that CRS neglects aquifer porosity and geothermal gradient, which results in the underestimation of aquifer temperature. The steady-state solution matches with the transient solution when the operating period reaches about 7×10^5 d. The temperature distributions of the aquicludes are affected by the geothermal gradient. In addition, the effect of the heat transfer coefficient on the aquiclude temperature distribution is appreciable only near the lower and upper boundaries of the aquicludes.

The present solutions can be applied to assess the effects of thermal properties, thickness of the storage aquifer, flow rate and operating time on spatial and temporal temperature distributions of the aquifer and the adjacent aquicludes in ATES systems. These solutions have practical use in designing an efficient ATES system for the injection of superfluous hot water into a confined aquifer as disposal storage of waste heat energy.

© 2010 The Authors, *GJI*, **183,** 237–251
Journal compilation © 2010 RAS

Downloaded from http://gji.oxfordjournals.org/ at National Chiao Tung University Library on April 24, 2014

ACKNOWLEDGMENTS

Research leading to this paper has been partially supported by 'Aim for the Top University Plan' of the National Chiao Tung University and Ministry of Education, Taiwan and the Taiwan National Science Council under the contract numbers NSC 99-NU-E-009-001 and NSC 99-2221-E-009-062-MY3. The authors thank the editor Prof Hort, the reviewer, Prof Sass, as well as three other anonymous reviewers for their constructive comments and valuable suggestions.

REFERENCES

Abramowitz, M. & Stegun, I.A., 1964. *Handbook of Mathematical Functions with Formulas, Graphs and Mathematical Tables,* National Bureau of Standards, Washington, Dover.

Bödvarsson, G.S. & Tsang, C.F., 1982. Injection and thermal breakthrough in fractured geothermal reservoirs, *J. geophys. Res.,* **87**(B2), 1031–1048.

Bödvarsson, G.S., Benson, S.M. & Witherspoon, P.A., 1982. Theory of the development of geothermal systems charged by vertical faults, *J. geophys. Res.,* **87**(B11), 9317–9328.

Bouhdjar, A. & Harhad, A., 2002. Numerical analysis of transient mixed convection flow in storage tank: influence of fluid properties and aspect ratios on stratification, *Renew. Energy,* **25,** 555–567.

Chen, C.S. & Reddell, D.L., 1983. Temperature distribution around a well during thermal injection and a graphical technique for evaluating aquifer thermal properties, *Water Resour. Res.,* **19**(2), 351–363.

Chen, J.S., Liu, C.W., Chen, C.S. & Yeh, H.D., 1996. A Laplace transform solution for tracer tests in a radially convergent flow field with upstream dispersion, *J. Hydrol.,* **183,** 263–275.

Crump, K.S., 1976. Numerical inversion of Laplace transforms using a Fourier series approximation, *J. Assoc. Comput. Mach.,* **23**(1), 89–96.

de Hoog, F.R., Knight, J.H. & Stokes, A.N., 1982. An improved method for numerical inversion of Laplace transforms, Society for Industrial and Applied Mathematics, *J. Sci. Stat. Comput.,* **3**(3), 357–366.

Ghassemi, A. & Kumar, G.S., 2007. Changes in fracture aperture and fluid pressure due to thermal stress and silica dissolution/precipitation induced by heat extraction from subsurface rocks, *Geothermics,* **36,** 115–140.

IMSL, 2003. IMSL Fortran Library User's Guide Math/Library Volume 2 of 2. version 5.0. Visual Numerics, Houston, Texas.

Nagano, K., Mochida, T. & Ochifuji, K., 2002. Influence of natural convection on forced horizontal flow in saturated porous media for aquifer thermal energy storage, *Appl. Therm. Eng.,* **22,** 1299–1311.

Özisik, M.N., 1993. *Heat Conduction,* 2nd edn, p. 29, John Wiley & Sons Inc, New York.

Sauty, J.P., Gringarten, A.C., Menjoz, A. & Landel, P.A., 1982a. Sensible energy storage in aquifers 1. Theoretical study, *Water Resour. Res.,* **18**(2), 245–252.

Sauty, J.P., Gringarten, A.C., Fabris, H., Thiery, D., Menjoz, A. & Landel, P.A., 1982b. Sensible energy storage in aquifers 2. Field experiments and comparison with theoretical results, *Water Resour. Res.,* **18**(2), 253–265.

Shanks, D., 1955. Non-linear transformations of divergent and slowly convergent sequences, *J. Math. Phys.,* **34,** 1–42.

Spiegel, M.R., 1965. *Schaum's Outline of Theory and Problems of Laplace Transforms,* Schaum, New York.

Yang, S.Y. & Yeh, H.D., 2007. On the solutions of modeling slug test performed in a two-zone confined aquifer, *Hydrogeol. J.,* **15**(2), 297–305.

Yang, S.Y., Yeh, H.D. & Chiu, P.Y., 2006. A closed-form solution for constant-flux pumping test under the effect of well partial penetration, *Water Resour. Res.,* **42**(5), 1–8.

Yeh, H.D. & Wang, C.T., 2007. Large-time solutions for groundwater flow problems using the relationship of small p versus large t, *Water Resour. Res.,* **43**(6), W06502.

Yeh, H.D. & Yang, S.Y., 2006. A novel analytical solution for a slug test conducted in a well with a finite-thickness skin, *Adv. Water Resour.,* **29**(10), 1479–1489.

Yumrutas, R. & Ünsal, M., 2005. Modeling of a space cooling system with underground storage, *Appl. Therm. Eng.,* **25,** 227–239.

APPENDIX A: DEVELOPMENT OF SOLUTIONS (15), (19) AND (20)

Eqs (1)–(14) can be expressed in dimensionless form using dimensionless parameters given in Table 1. The heat convection–conduction equation describing aquifer temperature distribution in dimensionless form may be expressed as

$$\frac{\partial^2 T_{aD}(R, Z_a, \tau)}{\partial R^2} + \left(\frac{1-2v}{R}\right)\frac{\partial T_{aD}(R, Z_a, \tau)}{\partial R} + \frac{\partial^2 T_{aD}(R, Z_a, \tau)}{\partial Z_a^2} + \lambda_{1D}\left.\frac{\partial T_{1D}(R, Z_1, \tau)}{\partial Z_1}\right|_{Z_1=0} + \lambda_{2D}\left.\frac{\partial T_{2D}(R, Z_2, \tau)}{\partial Z_2}\right|_{Z_2=0} = \frac{\partial T_{aD}(R, Z_a, \tau)}{\partial \tau} \tag{A1}$$

subject to following dimensionless forms of the initial and boundary conditions

$$T_{aD}(R, Z_a, 0) = -2T_{ag}Z_a \tag{A2}$$

$$T_{aD}(R_w, Z_a, \tau) = 1 \tag{A3}$$

$$T_{aD}(\infty, Z_a, \tau) = -2T_{ag}Z_a \tag{A4}$$

$$\frac{\partial T_{aD}(R, 0, \tau)}{\partial Z_a} = -2\frac{\partial T_{1D}(R, 0, \tau)}{\partial Z_1} \tag{A5}$$

and

$$\frac{\partial T_{aD}(R, 2, \tau)}{\partial Z_a} = 2\frac{\partial T_{2D}(R, 0, \tau)}{\partial Z_2}. \tag{A6}$$

The heat conduction equation describing temperature distribution in the underlying aquiclude can be written in dimensionless form as

$$\frac{\partial^2 T_{1D}(R, Z_1, \tau)}{\partial Z_1^2} = \frac{1}{\alpha_{1D}}\frac{\partial T_{1D}(R, Z_1, \tau)}{\partial \tau}, \quad 0 < Z_1 < 4B_1 \tag{A7}$$

where $\alpha_{1D} = 4\alpha_1/\alpha_a$ and $Z_1 = -4z/b_a$.

© 2010 The Authors, *GJI*, **183,** 237–251
Journal compilation © 2010 RAS

Downloaded from http://gji.oxfordjournals.org/ at National Chiao Tung Unive [redacted] on April 24, 2014

Subject to following dimensionless initial and boundary conditions

$$T_{1D}(R, Z_1, 0) = T_{1g} Z_1 \tag{A8}$$

$$T_{1D}(R, 0, \tau) = T_{aD}(R, Z_a, \tau) \tag{A9}$$

and

$$\frac{\partial T_{1D}(R, 4B_1, \tau)}{\partial Z_1} = -\frac{\beta_1}{4}\left[T_{1D}(R, 4B_1, \tau) - T_{10D}\right], \tag{A10}$$

where $T_{10D} = (T_{10} - T_{a0})/(T_{in} - T_{a0})$, $B_1 = b_1/b_a$ and $\beta_1 = h_1 b_a/\lambda_1$.

Similarly, the heat conduction equation describing temperature distribution in the overlying aquiclude in dimensionless form is

$$\frac{\partial^2 T_{2D}(R, Z_2, \tau)}{\partial Z_2^2} = \frac{1}{\alpha_{2D}} \frac{\partial T_{2D}(R, Z_2, \tau)}{\partial \tau}, \quad 0 < Z_2 < 4B_2 \tag{A11}$$

subject to following dimensionless initial and boundary conditions

$$T_{2D}(R, Z_2, 0) = -T_{2g}(Z_2 + 4) \tag{A12}$$

$$T_{2D}(R, 0, \tau) = T_{aD}(R, Z_a, \tau) \tag{A13}$$

and

$$\frac{\partial T_{2D}(R, 4B_2, \tau)}{\partial Z_2} = -\frac{\beta_2}{4}\left[T_{2D}(R, 4B_2, \tau) - T_{20D}\right], \tag{A14}$$

where $\alpha_{2D} = 4\alpha_2/\alpha_a$ $Z_2 = 4(z - b_a)/b_a$,$T_{20D} = (T_{20} - T_{a0})/(T_{in} - T_{a0})$, $B_2 = b_2/b_a$ and $\beta_2 = h_2 b_a/\lambda_2$.

Taking Laplace transforms of eqs (A1), (A3), (A4)–(A6) yield

$$\frac{d^2\overline{T}_{aD}(R, Z_a, p)}{dR^2} + \left(\frac{1-2v}{R}\right)\frac{d\overline{T}_{aD}(R, Z_a, p)}{dR} + \frac{d^2\overline{T}_{aD}(R, Z_a, p)}{dZ_a^2} + \lambda_{1D}\left.\frac{d\overline{T}_{1D}(R, Z_1, p)}{dZ_1}\right|_{Z_1=0} + \lambda_{2D}\left.\frac{d\overline{T}_{2D}(R, Z_2, p)}{dZ_2}\right|_{Z_2=0}$$
$$= p\overline{T}_{aD}(R, Z_a, p) + 2T_{ag} Z_a \tag{A15}$$

subject to

$$\bar{T}_{aD}(R_w, Z_a, p) = 1/p \tag{A16}$$

$$\bar{T}_{aD}(\infty, Z_a, p) = -2T_{ag} Z_a/p \tag{A17}$$

$$\frac{d\bar{T}_{aD}(R, 0, p)}{dZ_a} = -2\frac{d\bar{T}_{1D}(R, 0, p)}{dZ_1} \tag{A18}$$

and

$$\frac{d\bar{T}_{aD}(R, 2, p)}{dZ_a} = 2\frac{d\bar{T}_{2D}(R, 0, p)}{dZ_2}. \tag{A19}$$

Moreover, the heat conduction equation for the underlying aquiclude after taking Laplace transform of eq. (A7) yields

$$\frac{d^2\bar{T}_{1D}(R, Z_1, p)}{dZ_1^2} = q_1^2\bar{T}_{1D}(R, Z_1, p) - \gamma_1^2 Z_1. \tag{A20}$$

Taking Laplace transforms of eqs (A9) and (A10), respectively, lead to

$$\bar{T}_{1D}(R, 0, p) = \bar{T}_{aD}(R, Z_a, p) \tag{A21}$$

and

$$\frac{d\bar{T}_{1D}(R, 4B_1, p)}{dZ_1} = -\frac{\beta_1}{4}\bar{T}_{1D}(R, 4B_1, p) + \frac{\beta_1}{4p}T_{10D}, \tag{A22}$$

where $q_1^2 = p/\alpha_{1D}$ and $\gamma_1^2 = T_{1g}/\alpha_{1D}$.

Similarly, the heat conduction equation for the overlying aquiclude after taking Laplace transform of eq. (A11) is

$$\frac{d^2\bar{T}_{2D}(R, Z_2, p)}{dZ_2^2} = q_2^2\bar{T}_{2D}(R, Z_2, p) + \frac{1}{4}\gamma_2^2(Z_2 + 4). \tag{A23}$$

The results of Laplace transforms of eqs (A13) and (A14) are, respectively

$$\bar{T}_{2D}(R, 0, p) = \bar{T}_{aD}(R, Z_a, p) \tag{A24}$$

and

$$\frac{d\bar{T}_{2D}(R, 4B_2, p)}{dZ_2} = -\frac{\beta_2}{4}\bar{T}_{2D}(R, 4B_2, p) + \frac{\beta_2}{4p}T_{20D}, \tag{A25}$$

where $q_2^2 = p/\alpha_{2D}$ and $\gamma_2^2 = T_{2g}/\alpha_{2D}$.

Downloaded from http://gji.oxfordjournals.org/ at National Chiao Tung University Library on April 24, 2014

Eqs (A20) and (A23) are linear differential equations and can be solved by applying the superposition principle. Their solutions in Laplace domain include the general solution, $\overline{T}^{h}_{1D}$ and the particular solution, $\overline{T}^{p}_{1D}$. That is

$$\overline{T}_{1D} = \overline{T}^{h}_{1D} + \overline{T}^{p}_{1D}. \tag{A26}$$

The Laplace-domain solution of eq. (A20) for the underlying aquiclude is then obtained as

$$\overline{T}_{1D} = C_1 \cosh q_1 Z_1 + C_2 \sinh q_1 Z_1 + \frac{\gamma_1^2}{q_1^2} Z_1, \tag{A27}$$

where C_1 and C_2 are the undetermined constants. Substituting eq. (A27) into eqs (A21) and (A22) and taking some algebraic manipulations, the constants can then be determined as

$$C_1 = \bar{T}_{\mathrm{a}D}(R, Z_{\mathrm{a}}, p) \tag{A28}$$

and

$$C_2 = -\bar{T}_{\mathrm{a}D}(R, Z_{\mathrm{a}}, p) x_1 + \frac{y_1}{p}\left[\beta_1 T_{10D} - 4T_{1g}(1 + \beta_1 B_1)\right], \tag{A29}$$

where $x_1 = [4q_1 \sinh(4q_1 B_1) + \beta_1 \cosh(4q_1 B_1)]y_1$ and $y_1 = 1/[4q_1 \cosh(4q_1 B_1) + \beta_1 \sinh(4q_1 B_1)]$. Eq. (19) can be obtained by substituting the constants in eqs (A28) and (A29) into eq. (A27). Similarly, the Laplace-domain solution of the overlying aquiclude can be obtained as eq. (20) from eqs (A23), (A24) and (A25).

Substituting eqs (19) and (20) into eq. (A15), one obtains

$$\frac{d^2\overline{T}_{\mathrm{a}D}(R, Z_{\mathrm{a}}, p)}{\mathrm{d}R^2} + \left(\frac{1-2v}{R}\right)\frac{\mathrm{d}\overline{T}_{\mathrm{a}D}(R, Z_{\mathrm{a}}, p)}{\mathrm{d}R} - A(0, p)\overline{T}_{\mathrm{a}D}(R, Z_{\mathrm{a}}, p) + \frac{d^2\overline{T}_{\mathrm{a}D}(R, Z_{\mathrm{a}}, p)}{\mathrm{d}Z_{\mathrm{a}}^2} = \frac{1}{p}B(0, p) + 2T_{\mathrm{a}g}Z_{\mathrm{a}}, \tag{A30}$$

where the functions of $A(0,p)$ and $B(0,p)$ in eq. (A30) are, respectively, given as eqs (22) and (23). Furthermore, taking Fourier cosine transforms of eq. (A30) and substituting eqs (A18) and (A19) into (A30) yield

$$\frac{d^2\overline{T}^{*}_{\mathrm{a}D}(R, \zeta_{\mathrm{a}}, p)}{\mathrm{d}R^2} + \left(\frac{1-2v}{R}\right)\frac{\mathrm{d}\overline{T}^{*}_{\mathrm{a}D}(R, \zeta_{\mathrm{a}}, p)}{\mathrm{d}R} - A(\zeta_{\mathrm{a}}, p)\overline{T}^{*}_{\mathrm{a}D}(R, \zeta_{\mathrm{a}}, p) = \frac{1}{p}B(\zeta_{\mathrm{a}}, p), \tag{A31}$$

where the functions of $A(\zeta_{\mathrm{a}}, p)$ and $B(\zeta_{\mathrm{a}}, p)$ in eq. (A31) are given as eqs (17) and (18), respectively. Eq. (A31) is a linear differential equation and can also be solved by applying the superposition principle. The Laplace–Fourier domain solution of eq. (A31) including a general solution $\overline{T}^{*h}_{\mathrm{a}D}$ and a particular solution $\overline{T}^{*p}_{\mathrm{a}D}$ can be expressed as

$$\overline{T}^{*}_{\mathrm{a}D} = \overline{T}^{*h}_{\mathrm{a}D} + \overline{T}^{*p}_{\mathrm{a}D}. \tag{A32}$$

The homogeneous equation in eq. (A31) is a special form of Bessel equation and its general solution can be expressed as

$$\overline{T}^{*h}_{\mathrm{a}} = R^{v}\left[D_1 I_v\left(\sqrt{A(\zeta_{\mathrm{a}}, p)}R\right) + D_2 K_v\left(\sqrt{A(\zeta_{\mathrm{a}}, p)}R\right)\right], \tag{A33}$$

where D_1 and D_2 are the undetermined constants. The non-homogeneous equation in eq. (A31) can be easily solved and its particular solution is

$$\overline{T}^{*p}_{\mathrm{a}D} = -\frac{B(\zeta_{\mathrm{a}}, p)}{pA(\zeta_{\mathrm{a}}, p)}. \tag{A34}$$

Based on the superposition principle, the Laplace–Fourier domain solution can then be obtained after substituting eqs (A33) and (A34) into eq. (A32) as

$$\overline{T}^{*}_{\mathrm{a}D} = R^{v}\left[D_1 I_v\left(\sqrt{A(\zeta_{\mathrm{a}}, p)}R\right) + D_2 K_v\left(\sqrt{A(\zeta_{\mathrm{a}}, p)}R\right)\right] - \frac{B(\zeta_{\mathrm{a}}, p)}{pA(\zeta_{\mathrm{a}}, p)}. \tag{A35}$$

Substituting eq. (A35) into eqs (A16) and (A17), the constants can be determined as

$$D_1 = 0 \tag{A36}$$

and

$$D_2 = \frac{1}{p}\left(\frac{1}{R_{\mathrm{w}}}\right)^{v}\left[\frac{1}{K_v\left(\sqrt{A(\zeta_{\mathrm{a}}, p)}R_{\mathrm{w}}\right)}\right]\left[\frac{B(\zeta_{\mathrm{a}}, p)}{A(\zeta_{\mathrm{a}}, p)} + \frac{\sin(2\zeta_{\mathrm{a}})}{\zeta_{\mathrm{a}}}\right]. \tag{A37}$$

Eq. (15) can then be obtained after substituting the constants (A36) and (A37) into eq. (A35) and taking Fourier cosine inversion.

APPENDIX B: DEVELOPMENT OF EQ. (27)

The steady-state solution can be obtained from the transient solution by applying the Final-Value Theorem (Yeh & Wang 2007) as

$$T_{\mathrm{a}D}(R, Z_{\mathrm{a}}, \infty) = \lim_{p\to 0} p\bar{T}_{\mathrm{a}D}(R, Z_{\mathrm{a}}, p). \tag{B1}$$

Accordingly, substituting eq. (15) into eq. (B1) yields

$$T_{\mathrm{a}D}(R, Z_{\mathrm{a}}, \infty) = \lim_{p\to 0}\left\{\frac{1}{2}\bar{T}^{*}_{\mathrm{a}D}(R, 0, p) + \sum_{n=1}^{\infty}\bar{T}^{*}_{\mathrm{a}D}(R, \zeta_{\mathrm{a}}, p)\cos(\zeta_{\mathrm{a}}Z_{\mathrm{a}})\right\} \tag{B2}$$

Downloaded from http://gji.oxfordjournals.org/ at National Chiao Tung Unive[redacted] on April 24, 2014

with

$$\bar{T}^*_{aD}(R, \zeta_a, p) = \left(\frac{R}{R_w}\right)^v \left[\frac{K_v\left(\sqrt{A(\zeta_a, p)}R\right)}{K_v\left(\sqrt{A(\zeta_a, p)}R_w\right)}\right]\left[\frac{B(\zeta_a, p)}{A(\zeta_a, p)} + \frac{\sin(2\zeta_a)}{\zeta_a}\right] - \frac{B(\zeta_a, p)}{A(\zeta_a, p)}.$$

The hyperbolic functions given by Abramowitz & Stegun (1964, p. 85) are

$$\sinh(\varepsilon) = \varepsilon + \frac{\varepsilon^3}{3!} + \frac{\varepsilon^5}{5!} + \frac{\varepsilon^7}{7!} + \ldots, \quad (|\varepsilon| < \infty) \tag{B3}$$

$$\cosh(\varepsilon) = 1 + \frac{\varepsilon^2}{2!} + \frac{\varepsilon^4}{4!} + \frac{\varepsilon^6}{6!} + \ldots, \quad (|\varepsilon| < \infty). \tag{B4}$$

Set $\varepsilon_1 = (4q_1B_1)$ and $\varepsilon_2 = (4q_2B_2)$ and let $p \to 0$ for eqs (B3) and (B4), eqs (17) and (18) can be respectively rewritten as

$$A(\zeta_a, 0) = \lambda_{1D}\beta_1 x + \lambda_{2D}\beta_2 y + \zeta_a^2 \tag{B5}$$

and

$$B(\zeta_a, 0) = \frac{\sin(2\zeta_a)\alpha(0)}{\zeta_a} - (-1)^n\left[\beta(0) - 2T_{2g}\right] - 2a_1y_1 - 2T_{1g} \tag{B6}$$

with

$$\alpha(0) = -\lambda_{1D}xa_1 - \lambda_{2D}ya_2 - \lambda_{1D}T_{1g} + \lambda_{2D}T_{2g} + 4\lambda_{2D}T_{2g}\beta_2 y \tag{B7}$$

and

$$\beta(0) = \frac{2ya_2}{1 + 4\beta_2 y}, \tag{B8}$$

where $x = 1/(4 + 4\beta_1B_1)$ and $y = 1/(4 + 4\beta_2B_2)$. Substituting eqs (B5) and (B6) into eq. (B2), the steady-state solution of aquifer temperature in dimensionless form is obtained as eq. (27).

Downloaded from http://gji.oxfordjournals.org/ at National Chiao Tung University Library on April 24, 2014

APPENDIX C: NOTATION

Table C1 provides a list of all the notation used in this article.

Table C1. Notation used in this article.

b_i	thickness (m), $i = 1, 2$ or a
B_i	$= b_i/b_a$, $i = 1, 2$; dimensionless thickness
C_i	$= (\rho c)_i$, volumetric thermal capacity [J (m^3 K)$^{-1}$], $i = 1, 2$ or a
g_i	geothermal gradient (°C m^{-1}), $i = 1, 2$ or a
h_i	heat transfer coefficient [W (m^2 K)$^{-1}$], $i = 1, 2$
n	aquifer porosity, dimensionless
p	Laplace transform variable
q_i^2	$= p/\alpha_{iD}$, $i = 1, 2$
Q	injection flow rate (m^3 s^{-1})
r	radial distance from the centre of injection well (m)
r_w	injection well radius (m)
R	$= 2r/b_a$; dimensionless radial distance from the centre of the injection well
R_w	$= 2r_w/b_a$; dimensionless injection well radius
t	injection time (s)
T_i	temperature (°C), $i = 1, 2$, a or in
T_{iD}	$= (T_i - T_{a0})/(T_{in} - T_{a0})$, $i = 1, 2$, or a; dimensionless temperature
T_{ig}	$= g_i b_a/4(T_{in} - T_{a0})$, $i = 1, 2$, or a; dimensionless geothermal gradient
$\bar{T}_{iD}$	dimensionless temperature in Laplace domain, $i = 1, 2$ or a
$\bar{T}^*_{aD}$	dimensionless temperature in Fourier domain
u	volumetric flux per unit pore area (m s^{-1})
v	$= QC_a/4\pi n b_a \lambda_a$; dimensionless convective parameter
z	vertical distance from the bottom of the aquifer (m)
Z_a	$= 2z/b_a$; dimensionless vertical distance from the bottom of the aquifer in the aquifer
Z_1	$= -4z/b_a$; dimensionless vertical distance from the bottom of the aquifer in the underlying aquiclude
Z_2	$= 4(z - b_a)/b_a$; dimensionless vertical distance from the bottom of the aquifer in the overlying aquiclude
α_i	$= \lambda_i/C_i$, $i = 1, 2$ or a; thermal diffusivity (m^2 s^{-1})
α_{iD}	$= 4\alpha_i/\alpha_a$, $i = 1, 2$; dimensionless thermal diffusivity
β_i	$= h_i b_a/\lambda_i$, $i = 1, 2$; Biot number
γ_i^2	$= T_{ig}/\alpha_{iD}$, $i = 1, 2$
λ_i	thermal conductivity [W (m K)$^{-1}$], $i = 1, 2$ or a
λ_{iD}	$= \lambda_i/\lambda_a$, $i = 1, 2$; dimensionless thermal conductivity
ζ	Fourier transform variable
τ	$= 4\alpha_a t/b_a^2$; dimensionless injection time
Subscripts	
in	injection water
a	aquifer
0	reference value
1	underlying aquiclude
2	overlying aquiclude

Downloaded from http://gji.oxfordjournals.org/ at National Chiao Tung Unive[redacted] on April 24, 2014